Journal of Nuclear Materials 379 (2008) 133–141

Contents lists available at ScienceDirect

Journal of Nuclear Materials

journal homepage: www.elsevier.com/locate/jnucmat

Reactive-transport model for the prediction of the uniform corrosion behaviour of copper used fuel containers

F. King [a,*], M. Kolar [b], P. Maak [c]

[a] Integrity Corrosion Consulting Limited, Nanaimo, BC, Canada
[b] LS Computing, Nanaimo, BC, Canada
[c] Nuclear Waste Management Organization, Toronto, Ontario, Canada

A B S T R A C T

Used fuel containers in a deep geological repository will be subject to various forms of corrosion. For containers made from oxygen-free, phosphorus-doped copper, the most likely corrosion processes are uniform corrosion, underdeposit corrosion, stress corrosion cracking, and microbiologically influenced corrosion. The environmental conditions within the repository are expected to evolve with time, changing from warm and oxidizing initially to cool and anoxic in the long-term. In response, the corrosion behaviour of the containers will also change with time as the repository environment evolve. A reactive-transport model has been developed to predict the time-dependent uniform corrosion behaviour of the container. The model is based on an experimentally-based reaction scheme that accounts for the various chemical, microbiological, electrochemical, precipitation/dissolution, adsorption/desorption, redox, and mass-transport processes at the container surface and in the compacted bentonite-based sealing materials within the repository. Coupling of the electrochemical interfacial reactions with processes in the bentonite buffer material allows the effect of the evolution of the repository environment on the corrosion behaviour of the container to be taken into account. The Copper Corrosion Model for Uniform Corrosion predicts the time-dependent corrosion rate and corrosion potential of the container, as well as the evolution of the near-field environment.

1. Introduction

The Nuclear Waste Management Organization (NWMO) is developing the technology for the long-term management of Canada's used nuclear fuel. The NWMOs recommended approach, Adaptive Phased Management, was accepted by the Government of Canada on June 14, 2007. Adaptive Phased Management includes development of a deep geological repository (DGR) in a suitable rock formation such as the crystalline rock of the Canadian Shield or Ordovician sedimentary rock [1]. Fig. 1 shows a schematic of several different conceptual designs for a DGR in Canada [2].

Copper has been selected as the reference corrosion-barrier material for the used fuel container (UFC) in a potential DGR in a crystalline rock host formation [3]. Various container designs have been considered [4], but a possible configuration would involve the isolation of 324 used fuel bundles in a container comprising a carbon steel (C-steel) load-bearing vessel and an outer corrosion-barrier of oxygen-free, phosphorus-doped (OFP) copper (Fig. 2). OFP copper was developed in the Swedish program and is, essentially, oxygen-free copper (equivalent to UNS C10100) with the additional requirements of <5 ppm O, 50–70 ppm P, <0.6 ppm H, and <8 ppm S [5]. Phosphorus is added to improve the creep ductility of the material, and the H and S contents are minimized for the same reason. The oxygen specification was based on the need to avoid weld porosity using electron-beam welding, although friction stir welding is now the reference method for the final closure weld in Sweden.

2. The repository environment

A number of different options currently exist for the design of a deep geological repository for nuclear fuel waste in Canada (Fig. 1). The DGR would comprise a series of engineered and natural barriers, forming a multi-barrier system [2]. From the container outwards, these barriers could be: the wasteform itself, in the form of highly insoluble irradiated UO_2 pellets clad in a Zircaloy fuel sheath; the container; inner buffer material, consisting of compacted 100% bentonite clay; outer buffer material, a compacted 50:50 mixture of Na-bentonite clay and sand; dense backfill material, a compacted 70:30 mixture of crushed granite and bentonitic and glacial-lake clays; light backfill, a compacted mixture of

* Corresponding author. Tel.: +1 250 7511125, fax: +1 250 7511884.
E-mail address: fraser.king@shaw.ca (F. King).

0022-3115/$ - see front matter © 2008 Elsevier B.V. All rights reserved.
doi:10.1016/j.jnucmat.2008.06.017

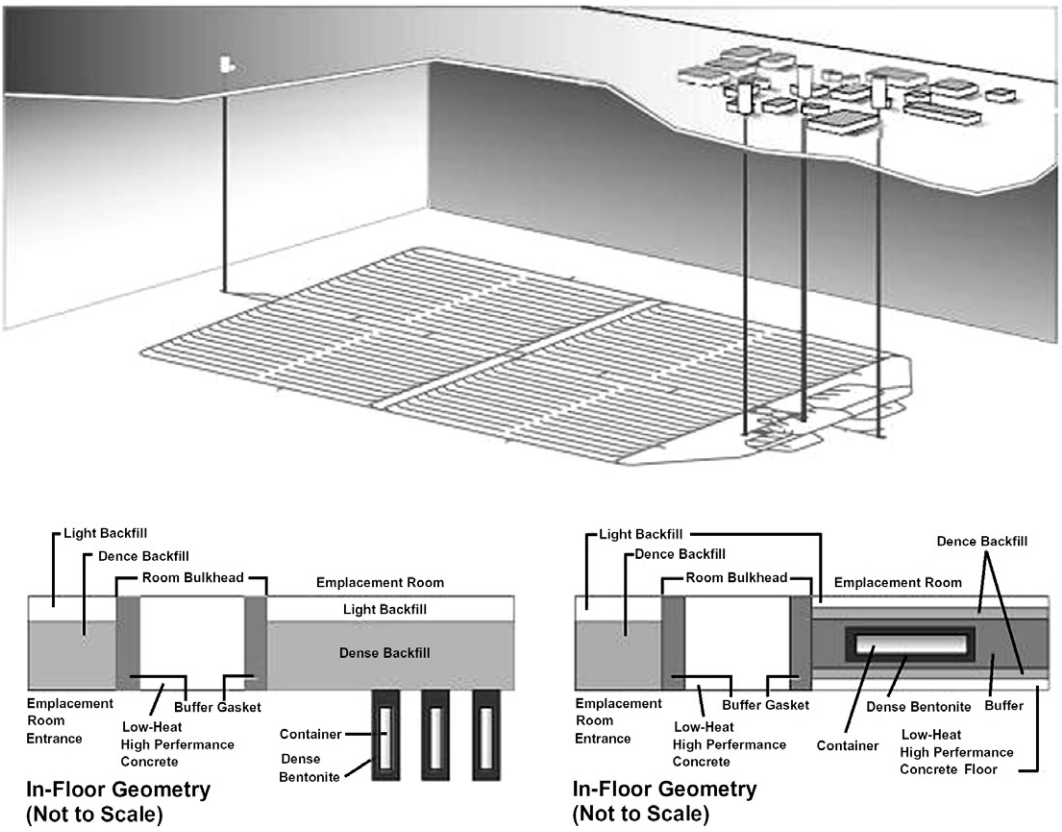

Fig. 1. Conceptual designs for a deep geological repository in Canada [2].

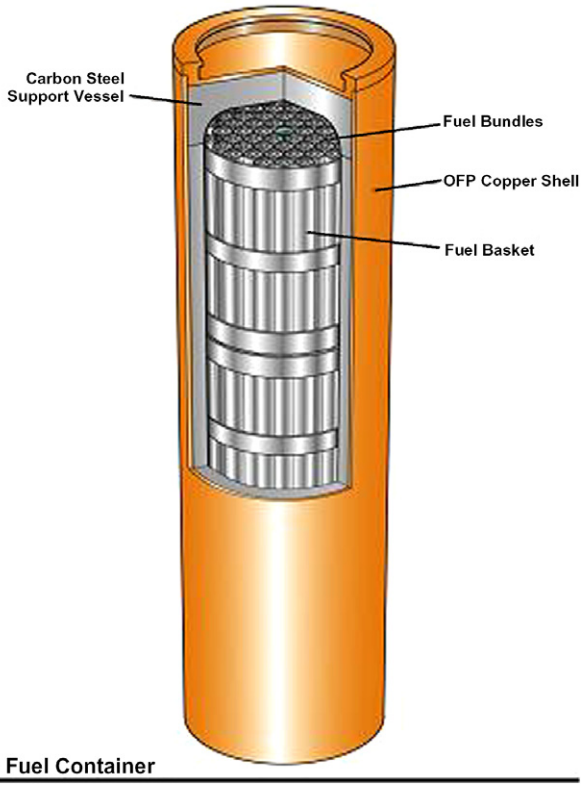

Fig. 2. Conceptual used fuel container design for 324 used fuel bundles comprising a carbon steel support vessel and outer OFP copper corrosion-barrier [4].

Na-bentonite and sand; the excavation-disturbed zone (EDZ) around he periphery of the tunnels and rooms, and the host rock itself. Both of the repository design options shown in Fig. 1 contain these various barriers, but differ in their orientation and placement.

From the viewpoint of the corrosion behaviour of Cu containers, the three most important environmental parameters in the DGR are the relative lack of oxidant, the restrictive mass-transport conditions, and the presence of saline groundwaters. The only significant source of oxidant is atmospheric O_2 trapped in the pores of the buffer and backfill materials as they are compacted and placed in the repository. Because of the low porosity of these materials, this trapped O_2 amounts to only 20–50 mol/container, depending upon the repository design. There are no other significant sources of oxidant because deep groundwaters are anoxic and the expected radiation dose rate at the surface of the container (<0.1 Sv h^{-1}) is too small to produce significant amounts of radical and molecular oxidizing species from the radiolysis of groundwater.

As well as limiting the amount of available oxidant, the compacted buffer and backfill materials also restrict the rate of mass-transport of species to and from the container. Transport occurs by diffusion only, with effective diffusion coefficients approximately 100 times lower than in bulk-solution [6]. Chloride is the dominant anion in deep groundwaters at potential repository locations, with concentrations typically in the range 0.1–5.0 mol dm^{-3} at depths of 500–1000 m [7]. Other significant environmental factors are the elevated container surface temperature (maximum ~90–100 °C) and the presence of an external load on the container (5–10 MPa from the 500–1000-m head of groundwater, up to 5 MPa from the swelling pressure of the buffer material, and 30 MPa hydrostatic pressure due to an assumed 3000-m-thick ice

sheet). The elevated temperature (T) will cause the buffer material closest to the container to partially desiccate initially, resulting in both liquid and vapour phases. The rate at which the buffer and backfill sealing materials saturate with groundwater, and hence the time at which the full external load is imposed on the container, will depend on the design of the repository and the properties of the surrounding rock.

An important aspect of the repository environment is that it will change over the extended periods of time of interest for nuclear waste management. Construction of the repository and emplacement of the heat-generating waste will disturb the benign conditions of the undisturbed rock formation. Slowly over time, the conditions in the DGR will evolve however, until eventually they resemble the conditions that prevailed prior to excavation. Thus, initial conditions will be warm and oxidizing because of heat output from the container and because of the presence of trapped atmospheric O_2. Conditions will become cooler and anoxic as the activity of the used fuel decreases and as the trapped O_2 is consumed by container corrosion, by reaction with oxidizable minerals (mainly Fe(II)-containing minerals) and other species in the buffer and backfill materials, and by microbial activity. This evolution of conditions is illustrated schematically in Fig. 3. Throughout this time, the Cl^- concentration in the buffer and backfill porewater will increase as Cl^- ions diffuse into the repository from the saline groundwater. Eventually, the conditions in the repository will be identical to those in the surrounding rock, i.e., an ambient temperature of ~10–15 °C, anoxic, saline ([Cl^-] in the range 0.1–5.0 mol dm^{-3}, depending upon repository depth and location), and water-saturated.

If sulphide ions are present, H_2O can also act as an oxidant for copper [8,9]. The model described here was developed to describe the corrosion behaviour of copper containers in a DGR in Canada. Neither the type of bentonite historically considered in Canada (Avonlea bentonite) nor the host crystalline rock of the Canadian Shield contain sulphide minerals. However, should a pyrite-containing bentonite be considered in the future, or if the Ordovician sedimentary deposits are shown to contain sulphide minerals, then the possibility of sulphide-induced corrosion would also need to be considered.

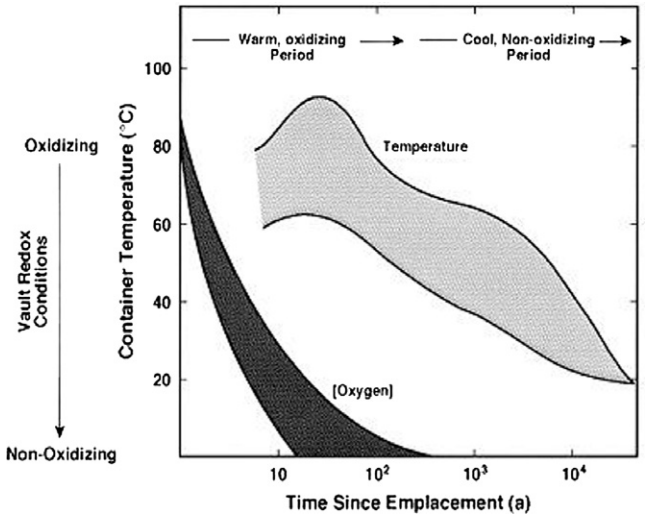

Fig. 3. Schematic illustrating the evolution of environmental conditions within a deep geological repository. As the trapped O_2 is consumed and the container surface temperature decreases, the repository environment will evolve from warm and oxidizing initially to an indefinite period of cool, anoxic conditions. At the same time, the pore-water salinity will increase as Cl^- diffuses in from the saline groundwater.

The corrosion behaviour of the containers will change with time as the environmental conditions within the repository evolve. In general, the initial warm, oxidizing period will be the most aggressive. Oxidant is available and temperatures are at their hottest. Once all the trapped O_2, and any Cu(II) species produced by container corrosion, have been consumed corrosion should cease since there will be no available oxidant to support corrosion. Therefore, provided Cu containers survive the initial warm, oxidizing period intact, they will become thermodynamically stable in the repository environment, ensuring virtually indefinite containment of the used fuel.

3. Corrosion behaviour of copper containers

Fig. 4 illustrates the mechanism proposed for the uniform corrosion of Cu in buffer and backfill materials in O_2-containing Cl^- environments [8–10]. This mechanism is based on the results of various experimental studies of the electrochemical and corrosion behaviour of Cu and of the properties of the clay-containing buffer and backfill. Various types of process are included in this mechanism: interfacial electron-transfer reactions, homogeneous redox reactions, precipitation/dissolution processes, adsorption/desorption, and mass-transport processes.

The interfacial electrochemical processes included in the mechanism have been studied in some detail. Based on our own work and that of others [11–13], the anodic dissolution of Cu in Cl^- solutions proceeds reversibly via an adsorbed $CuCl_{ADS}$ intermediate to produce dissolved $CuCl_2^-$ species (described by rate constants k_{af}, k_{ab}, k_{bf} and k_{bb} in Fig. 4). Oxygen reduction on Cu can be characterized as an irreversible 4-electron process producing OH^- (rate constant k_c), although the detailed mechanism depends on factors such as the interfacial pH and the presence of catalytic surface intermediates [14–16]. A combination of these two interfacial mechanisms accounts for the variation of the corrosion potential (E_{CORR}) of Cu in Cl^- solutions over a wide range of [O_2] and mass-transport conditions, including compacted clay [17]. As a consequence of the fact that both anodic and cathodic reactions are under transport control in compacted media, E_{CORR} is insensitive to the detailed interfacial mechanism for the reduction of O_2 [17]. The possibility of Cu(II) acting as an oxidant is also included in the mechanism through an irreversible interfacial reduction process (rate constant k_d). Because of the stabilization of Cu(I) by complexation with Cl^-, Cu does not undergo disproportionation in Cl^- environments [18].

Several homogeneous redox processes are included in the mechanism. Cupric species are formed from the oxidation of $CuCl_2^-$ by O_2 [19,20]

$$4CuCl_2^- + O_2 + 2H_2O \xrightarrow{k_1} 4Cu^{2+} + 8Cl^- + 4OH^-. \quad (1)$$

The rate of reaction is first-order with respect to both [$CuCl_2^-$] and [O_2], with the value of the rate constant k_1 increasing with T and pH, but inversely dependent on [Cl^-] because of the stabilization of Cu(I) as $CuCl_2^-$ complexes [19]. Cupric species, observed as dissolved and precipitated Cu(II) in corrosion experiments in compacted buffer [21], are formed exclusively by reaction (1), since it has been shown that Cu dissolves only as Cu(I) in Cl^- and Cl^-/SO_4^{2-} solutions over the range of potentials of interest [22]. The other homogeneous redox reactions in Fig. 4 involve Fe(II), formed by the dissolution of Fe(II)-containing minerals in the rock and clay, such as biotite (with the general formula $K(Mg_{0.6-1.8}Fe^{II}_{2.4-1.2})(Si_3Al)O_{10}(OH,F)_2$), magnetite, and pyrite. Dissolved Fe(II) reacts with either dissolved O_2 (rate constant k_5) or with Cu^{2+} (rate constant k_6). The reaction between Fe(II) and O_2 is pH-dependent and is first-order with respect to both [Fe(II)] and [O_2] [23]. The reaction with Cu^{2+} is assumed to be first-order with respect to [Fe(II)] and

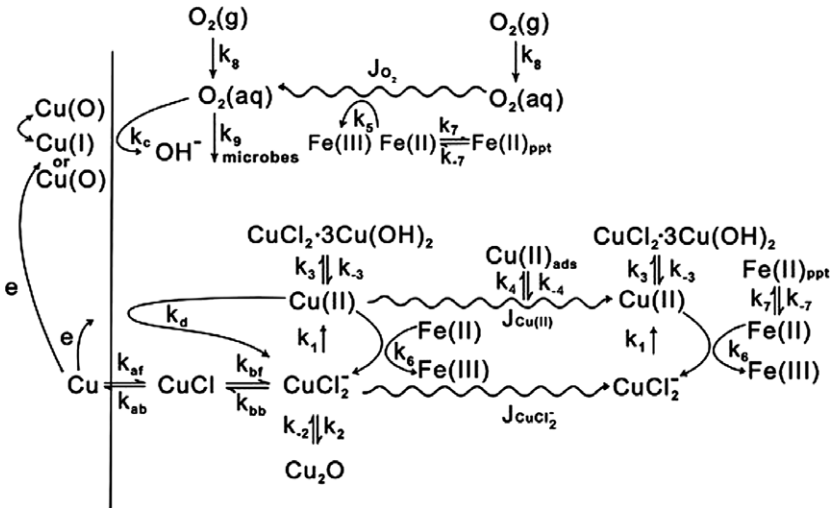

Fig. 4. Mechanism for the uniform corrosion of copper in compacted buffer and backfill materials saturated with O_2 containing saline groundwater. The J's and k's denote diffusive fluxes and rate constants for the various mass-transport, electrochemical, chemical, microbiological, precipitation/dissolution, adsorption/desorption and redox processes included in the mechanism.

$[Cu^{2+}]$. These latter processes are responsible for the expected evolution to anaerobic conditions in the repository.

The results of corrosion experiments in compacted buffer show the presence of precipitated Cu_2O and $CuCl_2$ $3Cu(OH)_2$ on the surfaces of Cu coupons [21]. Due to the high surface area:volume ratio in compacted media, precipitation may also occur on the clay, sand, and rock surfaces in the buffer and backfill. Precipitation of Cu_2O and $CuCl_2$ $3Cu(OH)_2$ (rate constants k_2 and k_3, respectively) is assumed to occur once the concentrations of $CuCl_2^-$ and Cu^{2+} exceed the solubilities of the respective solid phases for the particular conditions of $[Cl^-]$, T and pH under consideration. Re-dissolution of these phases is also included in the mechanism (rate constants k_{-2} and k_{-3}, respectively), at a rate which is dependent upon the surface area of the precipitated phase and pH, but not on $[Cl^-]$ [24]. Similarly, the precipitation and re-dissolution of a secondary Fe(II) phase is included in the mechanism (rate constants k_7/k_{-7}) to account for the accumulation of unreacted Fe(II). Ferrous species that react with either O_2 or Cu^{2+} are assumed to precipitate irreversibly as an Fe(III) solid.

Na-bentonite is a cation-exchanging mineral possessing a net negative surface charge [25]. Adsorption of dissolved Cu species has been shown to have a significant impact on the corrosion of Cu in compacted buffer material [21]. The extent of adsorption of Cu depends on its speciation, with cationic Cu(II) species (aquated Cu^{2+}, $CuOH^+$ or $CuCl^+$) strongly adsorbed but negatively charged $CuCl_2^-$ not adsorbed at all. Adsorption and desorption are described mechanistically using a kinetic Langmuir isotherm (rate constants k_4 and k_{-4}, respectively), with the rate of adsorption proportional to the number of vacant adsorption sites and the rate of desorption proportional to the number of occupied sites. Adsorption/desorption processes are frequently modelled using linear, equilibrium adsorption isotherms. However, the results of corrosion and adsorption experiments suggest that a Langmuir, rather than a linear, isotherm is more appropriate for the corrosion of Cu in compacted buffer material [21,26]. Furthermore, a comparison of the rates of adsorption/desorption with the transit time of diffusing species between adjacent adsorption sites suggests that equilibrium is unlikely to be established [6], as is frequently assumed.

The possibility of O_2-consumption by aerobic microbes is also included in the model (rate constant k_9 in Fig. 4). Although a more-detailed microbial model is available [27], the rate of aerobic respiration is treated here simply as a pseudo first-order process, with the value of the rate constant derived from the results of O_2-consumption in a long-term *in situ* test [28].

Mass-transport of solutes in buffer and backfill occurs by diffusion only. The hydraulic conductivities of the two materials are sufficiently low ($<10^{-10}$–10^{-12} m s^{-1}) as to preclude convective mass-transport. The double layer region adjacent to the randomly orientated clay, sand and rock surfaces do not cause migration of charged species [29]. Buffer and backfill materials can be described in terms of an equivalent porous medium, in which the effective diffusion coefficient (D_e) is given by [6,10,29,30]

$$D_e = \tau \varepsilon_e D_0, \tag{2}$$

where τ is the tortuosity factor, ε_e is the effective porosity for mass-transport and D_0 is the bulk-solution diffusion coefficient. Both τ

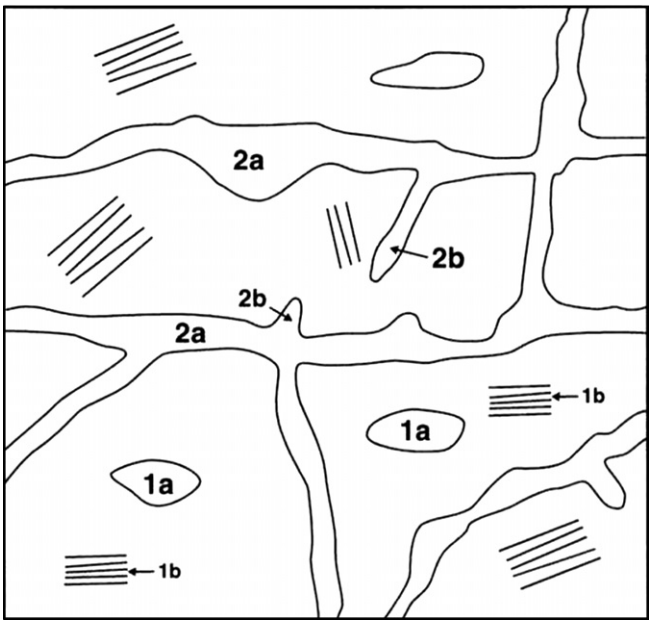

Fig. 5. Schematic illustrating the various types of pores in compacted buffer material. (1a) Isolated pores, (1b) pore volume associated with the inter-lamellar spaces between clay particles, (2a) through-pores for diffusive mass-transport, (2b) storage or dead-end pores.

and ε_e have values of ~0.1 for compacted buffer material [30]. Diffusion occurs through only part of the total porosity, that associated with through pores (denoted 2a in Fig. 5). The total porosity is composed of an accessible porosity, comprising through and dead-end pores (2a and 2b, respectively in Fig. 5), and an inaccessible porosity, comprising isolated pores and the pore space between clay and aggregate particles too small for diffusants to enter (1a and 1b, respectively). The total porosity depends on the compaction density, but it is divided approximately equally between accessible and non-accessible pores [31]. Because part of the pore volume is not accessible to diffusants, some of the trapped O_2 is not available to support corrosion and some of the adsorption sites will remain unoccupied. Consequently, the adsorption capacity of compacted clay is found to be less than that of unconsolidated material [31]. If the initially elevated temperature causes desiccation of the buffer, O_2 may partition into the vapour phase (rate constants k_8/k_{-8} in Fig. 4), resulting in rapid O_2 diffusion to the container surface [10].

The diffusion of Cu in compacted clay and buffer material has been studied in some detail. Copper concentration profiles were observed in corrosion experiments in which a Cu coupon was placed in contact with a column of compacted buffer material [21]. Although the time dependence of the interfacial [Cu] was not accurately known, it was possible to estimate values for the apparent diffusion coefficient of Cu(II) and Cu(I) (as non-sorbing anionic $CuCl_2^-$ species) (D_a) as a function of T [32].

4. Mathematical aspects of the copper corrosion model

The mathematical model is based on the corrosion model in Fig. 4 and a 1-dimensional (1-D), multi-layer description of the various mass-transport barriers surrounding the container (Fig. 6). An arbitray number of mass-transport layers can be included in the model representing, the inner and outer buffer material, light and dense backfill material, the EDZ, and the host rock. Each layer is described by its porosity and tortuosity factor, the content of Fe(II) minerals, and the time-dependent degree of saturation. A given material can be described by multiple layers in the model in order to provide a better description of the spatial dependence of the saturation front. The model is referred to as the Copper Corrosion Model for Uniform Corrosion (CCM-UC). Other variants of the model have been developed to predict the extent of microbiologically influenced corrosion (CCM-MIC) [27] and of stress corrosion cracking (CCM-SCC) [33], but are not discussed further here. A summary of the values of the electrochemical, precipitation/dissolution, adsoprtion/desorption, redox, and mass-transport input parameters is given in Appendix A. A description of the basis for these values is given by King and Kolar [9].

A series of reaction–diffusion equations is written for the various diffusing and non-diffusing species considered in the model, of the general form

$$\varepsilon_a \frac{\partial c}{\partial t} = \frac{\partial}{\partial x}\left(\varepsilon_e \tau D_0 \frac{\partial c}{\partial x}\right) + \varepsilon_a \sum_i R_i, \tag{3}$$

and

$$\frac{\partial c}{\partial t} = \varepsilon_a \sum_i R_i, \tag{4}$$

respectively, where c is the pore-water concentration, ε_a is the accessible porosity, and R_i describes the rates of the homogeneous reactions (denoted by rate constants k_1 through k_9 in Fig. 4). The 10 species considered in the model are (Fig. 4): dissolved O_2, O_2 in the gas-phase, dissolved Cu(I) (as $CuCl_2^-$), precipitated Cu(I) (as Cu_2O), dissolved Cu(II) (as Cu^{2+}), precipitated Cu(II) (as $CuCl_2 \cdot 3Cu(OH)_2$), adsorbed Cu(II), Cl^-, dissolved Fe(II), and precipitated Fe(II). In addition, a heat-conduction equation is included to simulate the effect of varying temperature within the repository.

The reaction–diffusion equations are solved using finite-difference techniques subject to a set of boundary and initial conditions. The boundary conditions (bc) for O_2, $CuCl_2^-$ and Cu^{2+} and Cl^- at $x = 0$ are defined by electrochemical expressions for the respective interfacial reactions shown in Fig. 4. These expressions are used to develop a mixed-potential model, enabling the corrosion potential (E_{CORR}) and corrosion rate (i_{CORR}) to be determined [17]. Dissolved Fe(II) is assigned a zero-flux bc at $x = 0$ and, since the remaining species do not diffuse, the respective mass-balance equations can be used as bc for these species. At the far boundary (the groundwater-bearing fracture), the diffusing Cu species are assigned a zero concentration bc, and O_2, Fe(II) and Cl^- have constant-concentration bc determined by the composition of the groundwater.

The initial conditions depend on the system being modelled. Invariably, the layers are taken to be initially free of all Cu species. In the example shown here, we assume time-dependent saturation of the various materials by incoming groundwater. The groundwater is assumed to be anoxic and to be saturated with Fe(II) (~10^{-5} mol dm^{-3}). The incoming groundwater is diluted by the fresh water used to compact the buffer and backfill materials. These materials are compacted at either 80% (buffer and dense backfill) or 33% (light backfill) of their saturated moisture contents. Therefore, there is significant air-filled void space in these layers. Oxygen partitions between the vapour and aqueous phases according to Henry's law.

In the simulations described here, a total of eleven mass-transport barriers were assumed, three for the inner buffer, two for the outer buffer, and one each for the light and dense backfill materials, the inner and outer EDZ, and the near- and far-field host rock. These layers are represented in the model by 725 grid points. The spacing of the grid points is determined by a geometrical progression, so that the points closest to the container, where the concentration profiles are generally the steepest, are closely spaced and the points further away become increasingly widely spaced. The

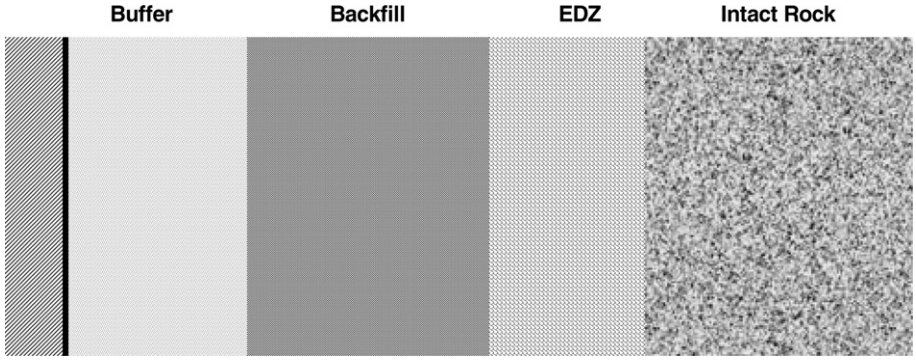

Fig. 6. Schematic representation of the series of 1-dimensional mass-transport barriers used in the model to simulate the various engineered and natural barriers.

smallest and largest grid spacings are of the order of 10 μm (at the container surface) and 2 m (in the rock layer). The size of the time increments is determined using an adaptive time-step algorithm which takes into account both the number of iterations required for convergence and the maximum change in concentration of any of the ten species in the previous time-step. Thus, small time-steps are used when concentrations are changing rapidly, as at short times, but when the concentration changes are small, longer intervals are used to minimize CPU time. The algorithm can handle abrupt changes in Δc encountered during the integration.

The output from the model includes the time-dependent values of E_{CORR} and i_{CORR}, and the concentrations of each of the ten chemical species as a function of distance and time. All other parameters are derived from these concentrations.

5. Model predictions

The CCM-UC was used to predict the uniform corrosion behaviour of copper UFC in a DGR in crystalline rock. Fig. 7 shows the predicted time dependence of E_{CORR} and i_{CORR} during the evolution of the repository environment. The rapid flux of O_2 to the container surface from the initially aerobic buffer material results in rapid corrosion initially, which then decreases as the O_2 supply diminishes. In fact, the major oxidant is Cu(II), formed from the homogeneous oxidation of Cu(I) by O_2. The increase in E_{CORR} is due to the increase in the interfacial concentration of $CuCl_2^-$ (see below).

Both E_{CORR} and i_{CORR} are undefined for periods between ~2 months and 100 years because, based on the assumed time dependence of the degree of saturation of the inner buffer material, the relative humidity at the container surface is predicted to be too low (<60%) to support electrochemical processes. Only once the container begins to cool and the buffer saturates does electrochemical activity, and hence corrosion, resume. By that time, however, the interfacial concentrations of O_2 and of Cu(II) are small and the corrosion rates are correspondingly low.

E_{CORR} is calculated from the i/E expression for the anodic reaction [9,17]

$$E_{CORR} = E_a^0 + \frac{2.3RT}{F}\log\left\{\frac{k_{ab}}{k_{af}k_{bf}[Cl^-]_0^2}\left(\frac{i_{CORR}}{nF} + k_{bb}[CuCl_2^-]_0\right)\right\}, \quad (5)$$

where E_a^0 is the standard potential for the anodic electron-transfer reaction, $[Cl^-]_0$ and $CuCl_2^-$ are the interfacial concentrations of Cl^- and $CuCl_2$ and n, F, R and T are the number of electrons transferred ($n = 1$), the Faraday constant, the gas constant and the absolute temperature, respectively. In general, E_{CORR} is a complex function of a number of time-dependent variables, including the interfacial concentrations of Cl^- and of $CuCl_2^-$ and temperature.

Fig. 8 shows the predicted time dependence of the integrated charge density for the anodic and two cathodic reactions considered in the model, expressed in terms of an equivalent thickness of copper. The total amount of corrosion is predicted to be <2 μm, with approximately equal amounts occurring before and after the container surfaces dries out. Of this corrosion, >99% is supported by the reduction of Cu(II) and only a small amount by the reduction of O_2.

The CCM-UC also predicts the speciation of the corroded copper as determined by the relative kinetics of the redox, precipitation/dissolution, and sorption/desorption processes. Fig. 9 shows the predicted time-dependent speciation of copper in terms of the spatially integrated amounts (in units of mol dm^{-2} as a result of the use of a 1-dimensional model) of dissolved $CuCl_2^-$, precipitated Cu_2O, dissolved Cu^{2+}, precipitated $CuCl_2$ $3Cu(OH)_2$, and adsorbed Cu(II). Up to a time of ~200 years, Cu(II) species predominate, with the majority of corroded Cu present in the system as Cu(II) adsorbed on the bentonite clay. This prediction is consistent with the results of laboratory corrosion experiments involving compacted bentonite in which steep Cu concentration profiles were observed in the clay adjacent to the copper surface [21]. At longer times, however, Cu(I) species predominate as both the O_2 and Cu(II) in the system are consumed by reaction with Fe(II) minerals and by corrosion of the container.

An important aspect of the evolution of the environment is the consumption of the initially trapped O_2 and the transition from aerobic to anaerobic conditions. In the CCM-UC, O_2 is consumed by (i) interfacial cathodic reduction on the container surface, (ii) the homogeneous oxidation of Cu(I) to Cu(II), (iii) reaction with Fe(II) minerals in the dense backfill, EDZ, and host rock, and (iv) aerobic microbial activity. Microbial activity is restricted to locations in the repository in which the water activity exceeds the threshold of 0.96 required to support metabolic processes [27,34,35]. Based on this criterion, microbial activity does not occur in the 100% bentonite inner buffer at any time, and only occurs in the outer buffer and backfill materials once the degree of saturation has increased following the initial desiccation, a period that varies between 27 and 71 years following closure of the repository, based on the assumed saturation characteristics.

Fig. 10 shows the predicted time dependence of the consumption of both gaseous and dissolved O_2. The model predicts a reduction in the initial O_2 inventory by five orders of magnitude after 57 years and by nine orders of magnitude after 200 years. Although there is no specific definition of the terms "anoxic" and "anaero-

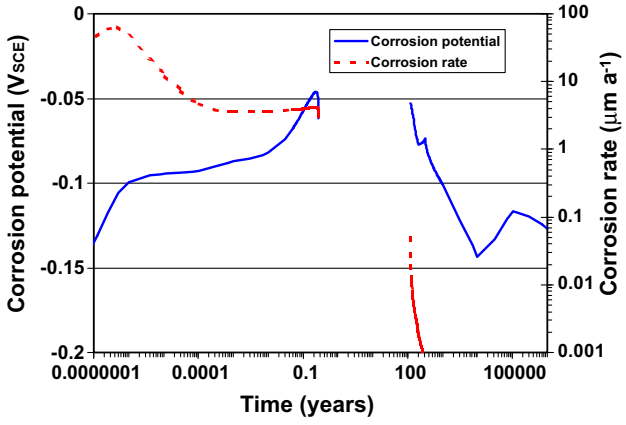

Fig. 7. Predicted time dependence of the corrosion potential and corrosion rate of copper used fuel containers.

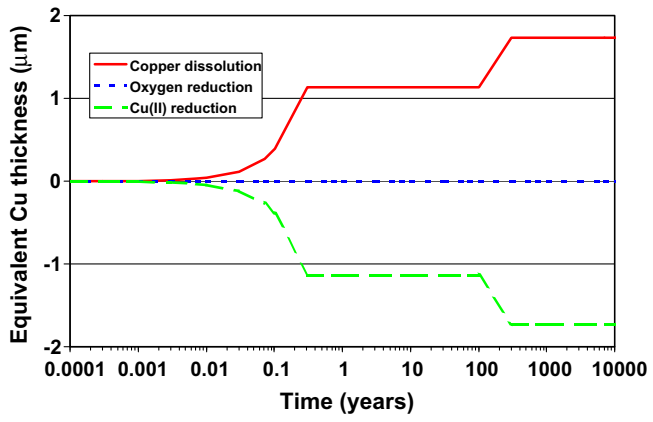

Fig. 8. Predicted time dependence of the integrated charge density for the anodic and cathodic processes, expressed in terms of an equivalent thickness of copper.

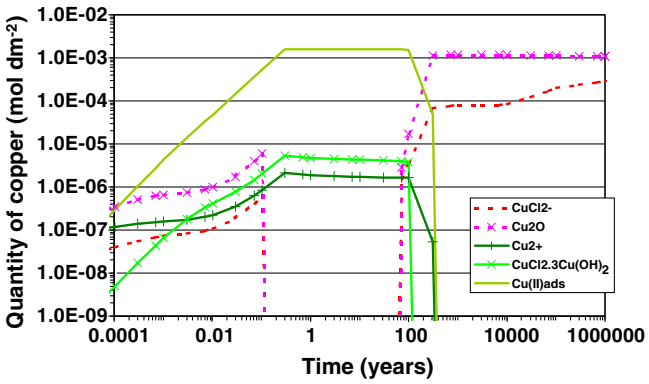

Fig. 9. Speciation of corroded copper as a function of time.

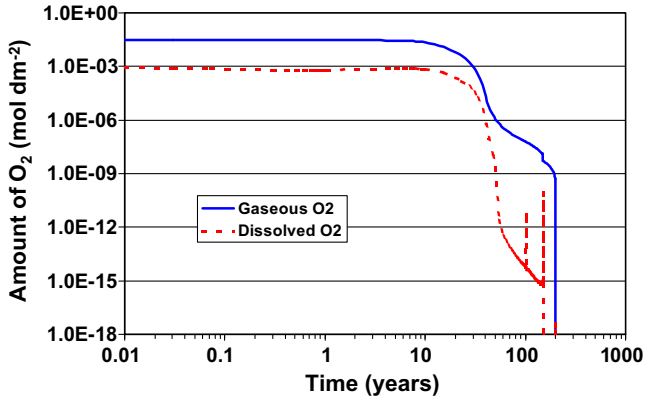

Fig. 10. Time-dependent consumption of the initial inventory of gaseous and dissolved oxygen in the repository.

bic", from a practical viewpoint, the establishment of anoxic conditions can be considered to occur somewhere between these two times. However, it should be noted that Cu(II) remains in the system for a period of 300–500 years after closure (Fig. 9), so the redox conditions near the container will remain "aerobic" for some time longer. (The "spikes" in the dissolved O_2 curve correspond to the times at which different layers are assumed to become fully saturated and the remaining gas-phase O_2 in the respective layers dissolves in the pore-water).

The spatial distribution of the amount of O_2 consumed by aerobic microbial activity is shown in Fig. 11. No microbial O_2-consumption occurs in the inner 100% bentonite buffer because of the low water activity in that material. However, increasing amounts of O_2 are consumed in the outer buffer, and dense and light backfill layers. The amount of O_2 consumed in each layer is a function of the inventory of O_2, which in turn is a function of the porosity and the initial degree of saturation, and the duration of microbial activity, which depends on the time at which the layer becomes sufficiently saturated to permit microbial activity. In this regard, microbial activity occurs earlier in the outer buffer and dense backfill materials (largely because of the higher initial degree of saturation in these layers), but the light backfill has a much greater initial inventory (72% of the total O_2 in the repository, compared with only ~6% in each of the outer buffer and dense backfill layers). Therefore, more O_2 is consumed by microbial activity in the light backfill than in either the outer buffer or dense backfill layers.

Another cause of O_2-consumption is reaction with ferrous ions released from Fe(II)-containing minerals in the sealing materials and host rock. (The current simulations were performed for a repository in granitic host rock, which contains several weight % biotite). Oxygen-consumption by redox reaction with Fe(II) occurs primarily in the EDZ and host rock and in the dense backfill, which is the only one of the sealing materials that contains crushed rock (Fig. 12). (Unlike other bentonites, the Avonlea bentonite specified here contains no pyrite, which would act as an additional source of Fe(II)). Although the EDZ contains a higher surface area of available Fe(II), the small pore volume limits the amount of O_2 available to be consumed. Some dissolved Fe(II) from the dense backfill layer diffuses into the adjacent outer buffer and light backfill, resulting in the "tails" of O_2-consumption in these layers apparent in Fig. 12. Furthermore, since the release of Fe(II) by biotite dissolution is temperature dependent, more O_2 is predicted to be consumed in the dense backfill closest to the container.

Fig. 13 shows an overall comparison of the time dependence of the various O_2-consumption reactions. For periods up to ~1–2 years, the main O_2-consumption reaction is the oxidation of Cu(I). However, once the buffer and backfill materials have saturated sufficiently to permit microbial activity, the consumption by aerobic microbes is predicted to predominate. Oxidation of Fe(II) also becomes an important cause of O_2-consumption later once the repository temperature has increased sufficiently to cause biotite alteration. Of the total inventory of O_2, 94% is predicted to be consumed by aerobic microbial activity, 3% by the oxidation of Cu(I), 4% by the oxidation of Fe(II), and <0.01% by the direct interfacial reduction reaction on the container surface. These fractions are, however, dependent on the values of the various rate constants used in the model. The rate of O_2-consumption by aero-

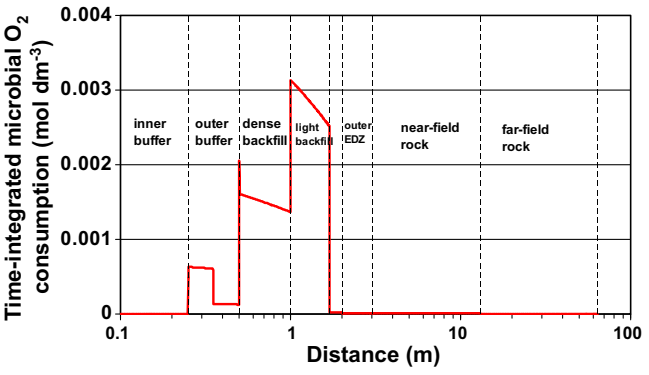

Fig. 11. Predicted spatial dependence of the contribution of microbial activity to the consumption of oxygen in the repository.

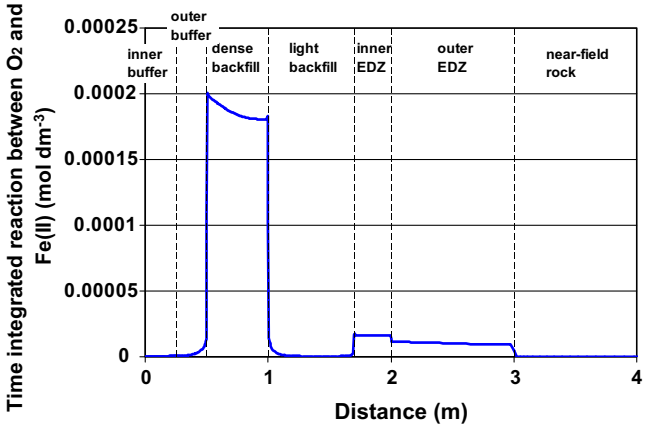

Fig. 12. Predicted spatial dependence of the contribution of redox reactions with ferrous minerals to the consumption of oxygen in the repository.

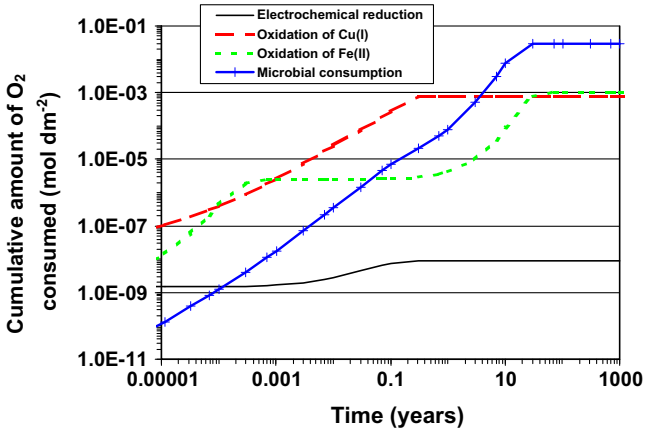

Fig. 13. Overall contributions of various processes to the consumption of oxygen during the evolution of the repository environment.

bic microbes in particular is uncertain, with the value for k_9 estimated from the results of a large-scale *in situ* test [28].

6. Conclusions

The corrosion behaviour of copper nuclear waste containers will change with time as the environmental conditions within the deep geological repository evolve, from warm and oxidizing initially to eventually cool and anoxic in the long-term. Containers that survive intact until the environmental conditions become benign can potentially provide indefinite containment of the nuclear fuel waste.

A 1-dimensional reactive-transport model has been developed to predict the long-term uniform corrosion behaviour of the container and the evolution of the repository environment. Interfacial electrochemical reactions on the container surface are coupled with chemical, microbiological, redox, adsorption/desorption, precipitation/dissolution, and mass-transport processes occurring in the various clay-based sealing materials and host rock. The model predicts the temporal and spatial variation of the concentrations of the various species included in the code, as well as the corrosion rate and the corrosion potential of the container.

The value of the model is not so much in the prediction of the corrosion rate, but more so in the insight that it provides regarding the coupling of the corrosion behaviour of the container to the evolution of the repository environment. In addition, the prediction of the corrosion potential allows the probability of other processes, such as localized corrosion and stress corrosion cracking, to be assessed.

Appendix A. Summary of electrochemical, mass-transport, and other kinetic data

k_1	rate constant for the homogeneous oxidation of $CuCl_2^-$ by O_2 (calculated within the model)
k_2	rate constant for the hydrolysis of $CuCl_2^-$ ($1\ s^{-1}$ at 25 °C)
ΔH_2	temperature dependence of k_2 ($60\ kJ\ mol^{-1}$)
k_{-2}	rate constant for the dissolution of Cu_2O ($0.1\ s^{-1}$ at 25 °C)
ΔH_{-2}	temperature dependence of k_{-2} ($40\ kJ\ mol^{-1}$)
k_3	rate constant for the precipitation of $CuCl_2\ 3Cu(OH)_2$ ($1 \times 10^{-5}\ s^{-1}$ at 25 °C)
ΔH_3	temperature dependence of k_3 ($60\ kJ\ mol^{-1}$)
k_{-3}	rate constant for the dissolution of $CuCl_2\ 3Cu(OH)_2$ ($1 \times 10^{-6}\ s^{-1}$ at 25 °C)
ΔH_{-3}	temperature dependence of k_{-3} ($60\ kJ\ mol^{-1}$)
k_4	rate constant for the adsorption of Cu^{2+} on Na-bentonite ($2 \times 10^{-3}\ dm^3\ mol^{-1}\ s^{-1}$ at 25 °C)
ΔH_4	temperature dependence of k_4 ($0\ kJ\ mol^{-1}$)
k_{-4}	rate constant for the desorption of Cu^{2+} ($1 \times 10^{-6}\ s^{-1}$ at 25 °C)
ΔH_{-4}	temperature dependence of k_{-4} ($0\ kJ\ mol^{-1}$)
k_5	rate constant for the reaction between O_2 and dissolved Fe(II) ($2.9\ dm^3\ mol^{-1}\ s^{-1}$ at 25 °C)
ΔH_5	temperature dependence of k_5 ($40\ kJ\ mol^{-1}$)
k_6	rate constant for the reaction between Cu^{2+} and Fe(II) ($10\ dm^3\ mol^{-1}\ s^{-1}$ at 25 °C)
ΔH_6	temperature dependence of k_6 ($40\ kJ\ mol^{-1}$)
k_7	rate constant for the rate of precipitation of an unidentified Fe(II) solid ($1.0\ s^{-1}$ at 25 °C)
ΔH_7	temperature dependence of k_7 ($60\ kJ\ mol^{-1}$)
k_{-7}	rate constant for the dissolution of a Fe(II) secondary phase ($0.1\ s^{-1}$ at 25 °C)
ΔH_{-7}	temperature dependence of k_{-7} ($60\ kJ\ mol^{-1}$)
k_8	rate constant for the dissolution of gaseous O_2 ($0.0122\ s^{-1}$ at 25 °C)
ΔH_8	temperature dependence of k_8 ($60\ kJ\ mol^{-1}$)
k_9	rate constant for the aerobic microbial consumption of O_2 ($2.2 \times 10^{-9}\ s^{-1}$ at 25 °C)
ΔH_9	temperature dependence of k_9 ($60\ kJ\ mol^{-1}$)
D_A	diffusion coefficient of gaseous O_2 in air ($0.00165\ dm^2\ s^{-1}$ at 25 °C)
ΔH_{D_A}	temperature dependence of D_A ($-2.06\ kJ\ mol^{-1}$ at 25 °C)
D_0	pore-solution diffusion coefficient of O_2 ($1.7 \times 10^{-7}\ dm^2\ s^{-1}$ at 25 °C)
ΔH_{D_0}	temperature dependence of D_0 ($15\ kJ\ mol^{-1}$)
D_1	pore-solution diffusion coefficient of $CuCl_2^-$ ($6 \times 10^{-8}\ dm^2\ s^{-1}$ at 25 °C)
ΔH_{D1}	temperature dependence of D_1 ($18.8\ kJ\ mol^{-1}$)
D_3	pore-solution diffusion coefficient of Cu^{2+} ($6 \times 10^{-8}\ dm^2\ s^{-1}$ at 25 °C)
ΔH_{D_3}	temperature dependence of D_3 ($15\ kJ\ mol^{-1}$)
D_6	pore-solution diffusion coefficient of Cl^- ($2 \times 10^{-7}\ cm^2\ s^{-1}$ at 25 °C)
ΔH_{D_6}	temperature dependence of D_6 ($15\ kJ\ mol^{-1}$)

D_7	pore-solution diffusion coefficient of Fe(II) (5×10^{-8} dm^2 s^{-1} at 25 °C)
ΔH_{D_7}	temperature dependence of D_7 (15 kJ mol^{-1})
c_1^{sat}	concentration of $CuCl_2^-$ in equilibrium with Cu_2O (3.4×10^{-3} mol dm^{-3} at 25 °C in 1 mol dm^{-3} Cl^-, pH 7)
ΔH_1^{sat}	temperature dependence of c_1^{sat} (24 kJ mol^{-1})
c_3^{sat}	concentration of Cu^{2+} in equilibrium with $CuCl_2$ $3Cu(OH)_2$ (4.3×10^{-7} mol dm^{-3} at 25 °C, pH 7)
ΔH_3^{sat}	temperature dependence of c_3^{sat} (19 kJ mol^{-1})
c_7^{sat}	concentration of dissolved Fe(II) in equilibrium with a precipitated Fe(II) secondary phase (1×10^{-5} mol dm^{-3} at 25 °C)
ΔH_7^{sat}	temperature dependence of c_7^{sat} (30 kJ mol^{-1})
F	Faraday constant (96 487 C mol^{-1})
R	gas constant (8.314 J K^{-1} mol^{-1})
n_0	number of electrons transferred in the reduction of O_2 (4)
α_{C1}	cathodic transfer coefficient for the reduction of O_2 (0.37)
k_c	electrochemical rate constant for the reduction of O_2 (1.7×10^{-9} dm s^{-1} at 25 °C)
ΔH_c	temperature dependence of k_c (60 kJ mol^{-1})
E_c^0	standard potential for the reduction of O_2 (0.16 V_{SCE} at 25 °C at pH 7)
ΔE_c^0	temperature dependence of E_c^0 (-1.23×10^{-4} V K^{-1})
n_a	number of electrons transferred during the oxidation of Cu (1)
E_a^0	standard potential for the dissolution of Cu as CuCl (-0.105 V_{SCE} at 25 °C)
ΔE_a^0	temperature dependence of E_a^0 (-6.35×10^{-4} V K^{-1})
k_a	combined electrochemical rate constant for the anodic dissolution of Cu (3.3×10^{-4} dm s^{-1} at 25 °C). k_a is a combined rate constant, equivalent to $k_{af}k_{bf}/k_{ab}$
ΔH_a	temperature dependence of k_a (60 kJ mol^{-1}).
k_{bb}	rate constant for the conversion of $CuCl_2^-$ to CuCl (1.42×10^{-3} dm s^{-1} at 25 °C)
ΔH_{bb}	temperature dependence of k_{bb} (60 kJ mol^{-1})
n_2	number of electrons transferred for the reduction of Cu^{2+} (1)
k_d	electrochemical rate constant for the reduction of Cu^{2+} (2×10^{-8} dm s^{-1} at 25 °C)
ΔH_d	temperature dependence of k_d (45 kJ mol^{-1})
α_d	transfer coefficient for the reduction of Cu^{2+} (0.5)
E_d^0	standard potential for the reduction of Cu^{2+} (0.223 V_{SCE} at 25 °C)
ΔE_d^0	temperature dependence of E_d^0 (0 V K^{-1})

References

[1] Choosing a way forward, The future management of Canada's used nuclear fuel, Final study, Nuclear Waste Management Organization, Toronto, Ontario, 2005.
[2] S.B. Russell, G.R. Simmons, Proceedings of the 10th International High-Level Radioactive Waste Management Conference, Las Vegas, NV, March 30–April 2, 2003, American Nuclear Society, La Grange Park, IL, 2003, p. 563.
[3] P. Maak, The selection of a corrosion-barrier primary material for used-fuel disposal containers, Ontario Power Generation, Nuclear Waste Management Division Report 06819-REP-01200-10020-R00, 1999.
[4] P. Maak, G. Simmons, Summary report: a screening study of used-fuel container geometric designs and emplacement methods for a deep geologic repository, Ontario Power Generation, Nuclear Waste Management Division Report 06819-REP-01200-10065-R00, 2001.
[5] C.-G. Andersson, P. Eriksson, M. Westman, G. Emilsson, Status report, canister fabrication, Swedish Nuclear Fuel and Waste Management Company Report, SKB TR 04-23, 2004.
[6] F. King, M. Kolar, D.W. Shoesmith, CORROSION/96, Paper #380, NACE International, Houston, TX, 1996.
[7] S.K. Frape, P. Fritz, R.H. McNutt, Geochim. Cosmochim. Acta 48 (1984) 1617.
[8] F. King, M. Kolar, in: W.M. Murphy, D. Knecht (Eds.), Scientific Basis for Nuclear Waste Management XIX, Mater. Res. Soc. Proc., vol. 412, 1996, p. 555.
[9] F. King, M. Kolar, The copper container corrosion model used in AECL's second case study, Ontario Power Generation, Nuclear Waste Management Division Report 06819-REP-01200-10041-R00, 2000.
[10] F. King, M. Kolar, CORROSION/95, Paper #425, NACE International, Houston, TX, 1995.
[11] C. Deslouis, B. Tribollet, G. Mengoli, M.M. Musiani, J. Appl. Electrochem. 18 (1988) 374.
[12] A. Moreau, Electrochim. Acta 26 (497–505) (1981) 1609.
[13] H.P. Lee, K. Nobe, J. Electrochem. Soc. 133 (1986) 2035.
[14] F. King, C.D. Litke, Y. Tang, J. Electroanal. Chem. 384 (1995) 105.
[15] F. King, M.J. Quinn, C.D. Litke, J. Electroanal. Chem. 385 (1995) 45.
[16] M.V. Vazquez, S.R. de Sanchez, E.J. Calvo, D.J. Schiffrin, J. Electroanal. Chem. 374 (1994) 189.
[17] F. King, C.D. Litke, M.J. Quinn, D.M. LeNeveu, Corros. Sci. 37 (1995) 833.
[18] D.G. Peters, S.A. Cruser, J. Electroanal. Chem. 9 (1965) 27.
[19] V.K. Sharma, F.J. Millero, J. Solution Chem. 17 (1988) 581.
[20] M.J. Nicol, S. Afr. J. Chem. 37 (1984) 77.
[21] F. King, C.D. Litke, S.R. Ryan, Corros. Sci. 33 (1992) 1979.
[22] F. King, Y. Tang, M.J. Quinn, C.D. Litke, CORROSION/95, Paper #424, NACE International, Houston, TX, 1995.
[23] B. Wehrli, in: W. Stumm (Ed.), Aquatic Chemical Kinetics, Wiley Interscience, New York, 1990. (Chapter 11).
[24] F. King, N. Légère, unpublished data.
[25] G. Sposito, The Chemistry of Soils, Oxford University Press, Oxford, 1989.
[26] S.R. Ryan, F. King, Atomic Energy of Canada Limited Report, AECL-11062, COG-I-94-125 (1994), Available from SDDO, Chalk River Laboratories, Chalk River, Ontario, Canada K0J 1J0.
[27] F. King, M. Kolar, S. Stroes-Gascoyne, P. Maak, in: (V.M. Oversby, L.O. Werme (Eds.), Scientific Basis for Nuclear Waste Management XXVII, Mater. Res. Soc. Symp. Proc., vol. 807, Materials Research Society, Warrendale, PA, 2004, p. 811.
[28] S. Stroes-Gascoyne, F. King, in: Proceedings of CORROSION/2002 Research Topical Symposium, NACE International, Houston, TX, 2002.
[29] D.W. Oscarson, Clays Clay Miner. 42 (1994) 534.
[30] D.W. Oscarson, H.B. Hume, N.G. Sawatsky, S.C.H. Cheung, Soil Sci. Soc. Am. J. 56 (1992) 1400.
[31] D.W. Oscarson, H.B. Hume, F. King, Clays Clay Miner. 42 (1994) 731.
[32] F. King, Appl. Geochem. 10 (1995) 477.
[33] P. Maak, F. King, in: P. Van Iseghem (Ed.), Scientific Basis for Nuclear Waste Management XXIX, Mater. Res. Soc. Symp. Proc., vol. 932, Materials Research Society, Warrendale, PA, 2005, p. 837.
[34] S. Stroes-Gascoyne, C.J. Hamon, D.A. Dixon, C. Kohle, P. Maak, in: Darrell Dunn, Christophe Poinssot, Bruce Begg (Eds.), Scientific Basis for Nuclear Waste Management XXX, Mater. Res. Soc. Symp. Proc., vol. 985, Warrendale, PA, 2007, Paper 0985-NN13-02.
[35] F. King, in: Proceedings of 2008 Research Topical Symposium, CORROSION/2008, NACE International, Houston, TX, 2008.